PROCEEDINGS OF SCIENCE

Detecting the Next Galactic Core-Collapse Supernova with TRIDENT

Ruike Cao,[a,*] **Iwan Morton-Blake,**[a] **Donglian Xu**[a,b,c] **and Yong-Zhong Qian**[d]

[a] *State Key Laboratory of Dark Matter Physics, Tsung-Dao Lee Institute, Shanghai Jiao Tong University, Shanghai 201210, China*

[b] *School of Physics and Astronomy, Shanghai Jiao Tong University, Shanghai 201210, China*

[c] *Hainan Research Institute, Shanghai Jiao Tong University, Hainan, China*

[d] *School of Physics and Astronomy, University of Minnesota, Minneapolis, MN 55455, USA*

E-mail: ruike_cao@sjtu.edu.cn

Large neutrino telescopes offer unique opportunities in detecting neutrinos from the next core-collapse supernova (CCSN), following the first and only detection in 1987. The TRopIcal DEep-sea Neutrino Telescope (TRIDENT) is a next-generation neutrino telescope to be built in the South China Sea. Although primarily designed for high-energy neutrino detection, TRIDENT could register a high flux of MeV-scale neutrinos from a nearby CCSN, causing a sudden rise of noise level from inverse beta decay (IBD) events induced by electron antineutrinos from the CCSN. TRIDENT's pixelized digital optical modules allow for a high-purity isolation of coincident pairs of signals from the prompt positron and delayed neutron events associated with IBD. The presence of chlorine in seawater is especially expected to boost the detection efficiency of neutrons. In this work, we present the study on TRIDENT's CCSN detection efficiency and alert time latency for a variety of CCSN models and distances.

39th International Cosmic Ray Conference (ICRC2025)
15–24 July 2025
Geneva, Switzerland

*Speaker

PoS(ICRC2025)1004

1. Core-Collapse Supernova Neutrinos

A core-collapse supernova (CCSN) occurs when the core of a massive star collapses into a proto-neutron star (PNS). Nearly all the gravitational binding energy ($\sim 10^{53}$ erg) of the PNS is emitted in ν_e, $\bar{\nu}_e$, ν_μ, $\bar{\nu}_\mu$, ν_τ, and $\bar{\nu}_\tau$ of $\sim$ 10–20 MeV [1]. These neutrinos are dominantly produced by electron and positron capture on free nucleons ($e^- + p \rightarrow n + \nu_e$, $e^+ + n \rightarrow p + \bar{\nu}_e$) and nucleon Bremsstrahlung ($N + N \rightarrow N + N + \nu + \bar{\nu}$) [2].

To date,only the neutrinos from a single CCSN, SN1987A in the Large Magellanic Cloud (~51.4 kpc away) have been detected. On 23 February 1987, ~20 $\bar{\nu}_e$ events at ~10 MeV were recorded, preceding the optical discovery of SN1987A [3]. These observations provided constraints on neutrino properties such as mass, magnetic moment, flavor oscillations, and decay. While tensions between models and observations remain [4], high-statistics measurements for the next Galactic CCSN by next-generation neutrino detectors are expected to provide detailed insights into CCSN neutrinos, potentially differentiating various models [5–7].

2. CCSN detection by neutrino telescopes

High-energy neutrino telescopes aim to probe astrophysical sources and production mechanisms of these neutrinos. Operating in the ~100 GeV–100 PeV regime, detectors such as IceCube, KM3NeT, and Baikal-GVD deploy digital optical modules (DOMs) across cubic-kilometer volumes with ~100 m spacing. The proposed TRIDENT telescope exemplifies next-generation designs [8], featuring hybrid DOMs (hDOMs) with multiple photomultiplier tubes (PMTs) and silicon photomultipliers (SiPMs) per module [9]. Its $\sim 8\,\mathrm{km}^3$ seawater volume and advanced photon detection capabilities aim to achieve unprecedented sensitivity to astrophysical neutrinos across all flavors.

The primary backgrounds of neutrino telescopes include atmospheric muons, radioactivity, and photodetector dark noise. With an elevated ^{40}K decay rate in seawater environments [10, 11], sensitivity to MeV-scale neutrinos is limited.

Despite the inherent limitations, CCSN neutrino bursts can induce a collective increase in single-DOM noise, enabling detection even in high-background environments [12]. This method has been implemented in IceCube [13, 14], IceCube-Gen2 [15], KM3NeT [16], Baikal-GVD [17], and other detectors, primarily targeting $\bar{\nu}_e$ via inverse beta decay (IBD):

$$\bar{\nu}_e + p \rightarrow e^+ + n\,. \tag{1}$$

In each IBD event, the ~15 MeV positron is accompanied by a thermalized neutron, typically captured on Hydrogen with a ~200 µs delay. Although 2.2 MeV γ-rays from such captures are challenging to detect in Cherenkov media, neutron tagging has been achieved in ultra-pure water [18]. The presence of chlorine (e.g., ^{35}Cl) in seawater offers an additional channel for neutron detection, with higher capture cross sections and yielding 8.6 MeV γ emissions [19]. We demonstrate that natural seawater composition can enhance neutron detection efficiency, thereby increasing IBD coincidence identification and CCSN sensitivity. While this study uses the TRIDENT configuration, the methods are generally applicable to seawater-based neutrino telescopes.

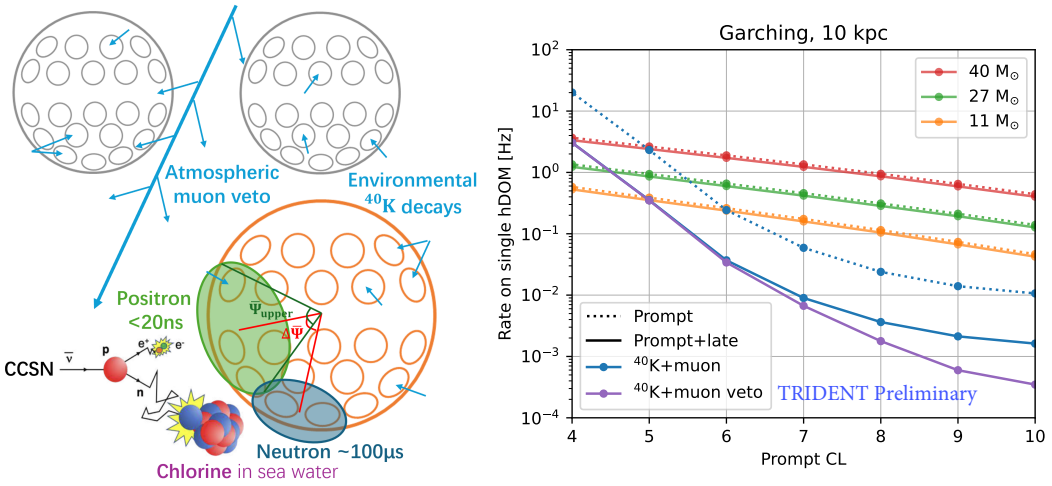

Figure 1: *Left*: Schematic of CCSN IBD signal extraction methods in seawater-based neutrino telescopes. See text for details. *Right*: Expected signal rate on single hDOM with different prompt CL cut, for various models of a CCSN at 10 kpc. Also shown are ^{40}K and atmospheric muon background rates before cut, with neutron filter (with $\bar{\Psi}$ cut), and with muon veto.

3. CCSN IBD signal extraction

The IBD interaction density within TRIDENT is:

$$\rho_{\mathrm{IBD}}(E_{e^+}) = \sigma(E_{\bar{\nu}_e}) F(E_{\bar{\nu}_e}) n_{\mathrm{H}}, \tag{2}$$

where $E_{e^+} = E_{\bar{\nu}_e} - 1.293$ MeV is the positron energy, $\sigma(E_{\bar{\nu}_e})$ is the IBD cross section [20], $F(E_{\bar{\nu}_e})$ is the expected $\bar{\nu}_e$ flux spectra from CCSN models (e.g., from the Garching group [21]), and n_{H} is the proton number density. For a 27 $\mathrm{M}_\odot$ progenitor at 10 kpc, the typical IBD interaction density is $\sim 0.1\,\mathrm{m}^{-3}$. This signal must be extracted amid substantial backgrounds, primarily ^{40}K β-decay in seawater and glass, PMT dark noise (1 kHz per PMT), and atmospheric muons [22], the last of which is modeled using MUPAGE [23].

To isolate IBD events, we utilize multiple selection strategies. The coincidence level (CL)—number of PMTs firing within 20 ns—suppresses low-energy backgrounds [24, 25]. Prompt positrons from IBD have higher CLs compared to ^{40}K events, enabling a CL threshold (e.g., CL ≥ 9) to distinguish signal (right panel of Fig. 1).

Neutron capture provides temporal correlation to enhance the signal-to-noise ratio (SNR). In seawater, ^{35}Cl (0.25% by abundance) has a large cross section (43.6 b) and emits 8.6 MeV gammas, yielding faster captures ($\sim 100\,\mu$s) and enhanced photon yield (Fig. 2, Table 1). These features improve tagging of delayed neutron signals.

Leveraging the pixelized design of TRIDENT's hDOMs, we calculate the angular spread $\bar{\Psi}$ of photon hits as:

$$\cos\Psi = \sin\theta_1 \sin\theta_2 \cos(\phi_1 - \phi_2) + \cos\theta_1 \cos\theta_2. \tag{3}$$

For multiple PMTs, the average angular spread $\bar{\Psi}$ is calculated as the mean angular distance between all PMT pairs. IBD positrons tend to yield $\bar{\Psi}$ of 40°–100°, whereas atmospheric muons have a

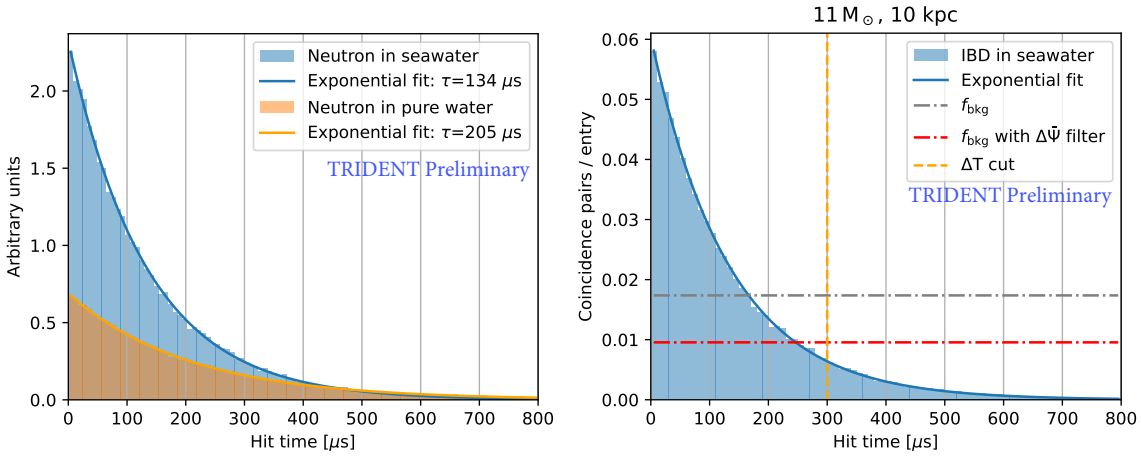

Figure 2: *Left*: Time distribution of detected photons from simulated 100 keV neutrons in sea water and pure water. Hit times represent the photon arrival times since the generation time of the neutron. *Right*: Expected signal rate on single hDOM with different prompt CL cut, for various models of a CCSN at 10 kpc. Also shown are ^{40}K and atmospheric muon background rates before cut, with neutron filter (with $\bar{\Psi}$ cut), and with muon veto.

broader range. A cut of $\bar{\Psi} < 80°$ retains >80% of IBD signals while rejecting ~70% of muons. Additionally, spatial alignment of positron-neutron pairs is enforced via $\Delta\bar{\Psi} < 100°$.

To further suppress muons, we apply an inter-hDOM muon veto: if two neighboring hDOMs (separation < 120 m) register CL≥ 2 within 150 ns, the event is vetoed. This rejects > 80% of muons with negligible impact on IBD signals.

All cuts are summarized in Table 2. Their cumulative effect is shown in Figs. 1 and 2, where signal-to-background ratio improves by ~10 times post-selection. A prompt-delayed coincidence time window of 0.3 ms is adopted, optimizing both background rejection and signal retention.

4. CCSN alert detection in TRIDENT

Combining coincident filtering with TRIDENT's full detector geometry, we assess its sensitivity to CCSNe via two approaches. First, we use Asimov datasets to estimate the detection

Table 1: Dominant nuclei for neutron capture in sea water, along with their number fractions (n), neutron capture cross sections (σ) and average gamma-ray energies ($\bar{E}_\gamma$). Data from NNDC [26].

Nuclei	n (number fraction)	$\bar{E}_\gamma$ [MeV]	σ [barn]
^{1}H	66.1%	2.22	0.333
^{16}O	33.2%	4.14	0.0002
^{23}Na	0.28%	6.96	0.52
^{35}Cl	0.25%	8.58	43.6
^{37}Cl	0.08%	6.11	0.43
^{24}Mg	0.03%	7.33	0.054

Table 2: Summary of coincidence cuts for IBD signal extraction and CCSN alerts.

Parameter	Prompt	Late
CL_{low}: Lower CL limit	9	2
$\bar{\Psi}_{upper}$: Maximum angular spread	80°	–
ΔT: Maximum prompt-delayed time difference	0.3 ms	
$\Delta\bar{\Psi}$: Maximum prompt-delayed angle	100°	
ΔT_{veto}: Time difference veto for nearby hDOMs with CL⩾2	150 ns	
N: Minimum number of hDOMs with IBD candidates in 1s	4 (25) for 200 (20k) hDOMs	

significance Z:

$$Z = \sqrt{2\left[(n_s + n_b)\ln\left(1 + \frac{n_s}{n_b}\right) - n_s\right]}, \tag{4}$$

where n_s and n_b are the expected signal and background counts in a 1-second window, aligned with the CCSN $\bar{\nu}_e$ burst duration. TRIDENT Phase-1 (200 hDOMs) achieves $Z \geq 5$ for 11 $M_\odot$ progenitors at 10 kpc, while the full array (20k hDOMs) extends the same detection significance to 60 kpc (Fig. 3).

Next, we implement a sliding window algorithm to define a real-time alert system. An alert is triggered when the number of hDOMs with IBD candidates within 1 s exceeds a threshold N. The false alert rate (FAR) is constrained to < 1/week. We find $N = 4$ sufficient for TRIDENT Phase-1, and $N = 25$ for the full detector (Table 2). Alert efficiencies are shown in Fig. 3, with comparison to other CCSN neutrino observatories.

Furthermore, the alert time—corresponding to the position of the triggering window—offers millisecond-level resolution. For TRIDENT Phase-1, Fig. 4 shows average trigger delays between $\sim$ 10 and 20 ms relative to the CCSN core bounce time for 11 $M_\odot$ and 27 $M_\odot$ progenitor models. The delays decrease to below 10 ms for the full detector.

5. Discussion and Conclusions

This study presents a novel IBD coincidence-based strategy for detecting CCSN neutrinos with undersea Cherenkov telescopes. The approach leverages high-density PMT designs and intrinsic seawater composition to identify MeV-scale $\bar{\nu}_e$ events despite high ambient noise. In TRIDENT, both Phase-1 and full-scale configurations are shown to achieve competitive sensitivities and alert capabilities, with broad applicability to other seawater-based detectors.

Rapid alerts from neutrino detectors provide essential lead time for electromagnetic and gravitational-wave follow-up. Precise timing of the rising edge enables discrimination among CCSN models [30], constrains the neutrino mass hierarchy [31], and allows for triangulation-based localization [32]. The synergy between neutrino telescopes and low-energy detectors will be critical in the multi-messenger era of CCSN observation.

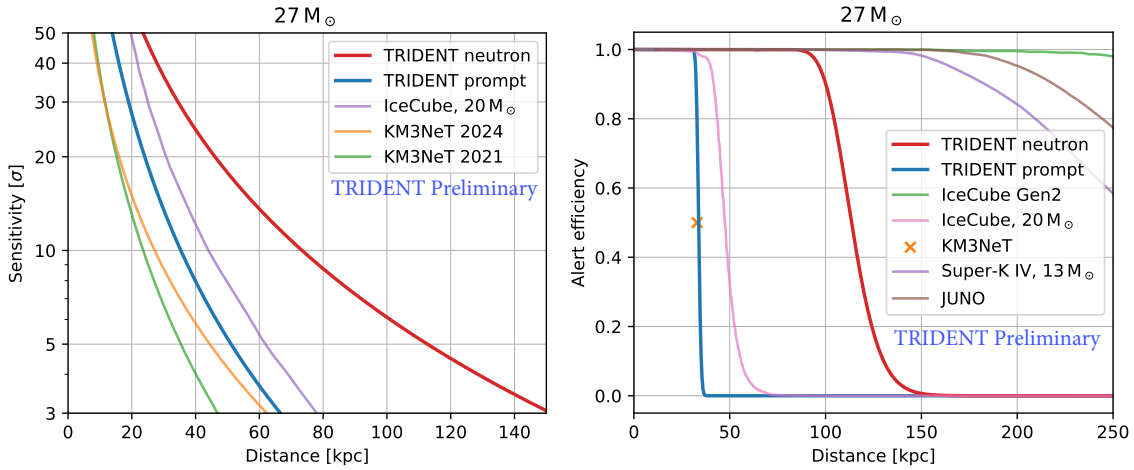

Figure 3: Comparison of CCSN neutrino sensitivity (*left*) and alert efficiency (*right*) as a function of distance, for a 27 $M_\odot$ Garching model (TRIDENT and KM3NeT [16, 27]). A 20 $M_\odot$ Lawrence-Livermore model is used for IceCube [13] and a 13 $M_\odot$ model (normal neutrino mass ordering, NO) is used for Super-Kamiokande [28]. Alert criteria are chosen to satisfy FAR $< 1/$week except for IceCube-Gen2 [15] with FAR $= 0.4/$year and JUNO (NO) [29] with FAR $= 1/$month.

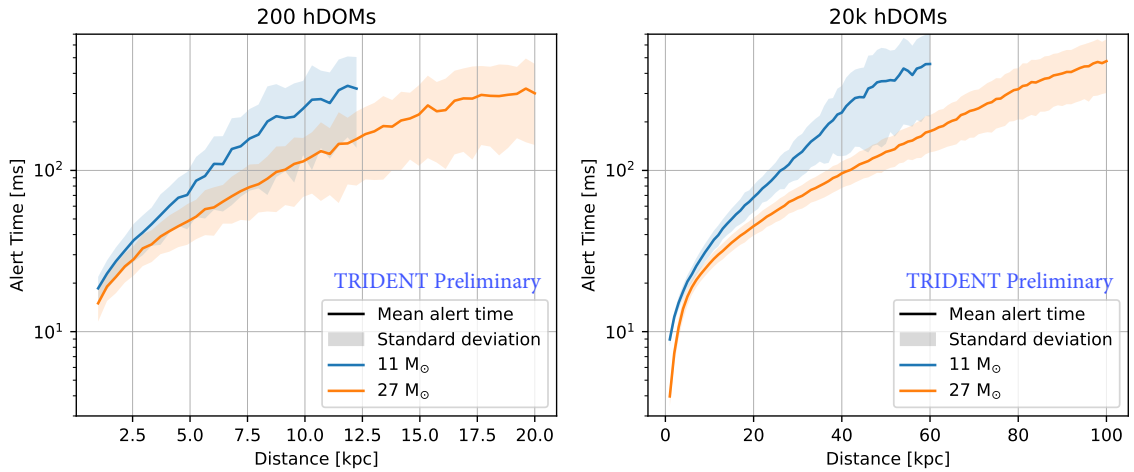

Figure 4: Average alert time as a function of CCSN distance, for 11 $M_\odot$ and 27 $M_\odot$ Garching models. Alert parameters are given in Table 2.

Acknowledgment

This work has received support from Ministry of Science and Technology of China under Grant No. 2022YFA1605500, the Office of Science and Technology of the Shanghai Municipal Government under Grant No. 22JC1410100 and National Natural Science Foundation of China Grant No. 123504104999.

References

[1] B. Müller. Neutrino Emission as Diagnostics of Core-Collapse Supernovae. *Ann. Rev. Nucl. Part. Sci.*, 69:253–278, 2019.

[2] Alessandro Mirizzi, Irene Tamborra, Hans-Thomas Janka, Ninetta Saviano, Kate Scholberg, Robert Bollig, Lorenz Hudepohl, and Sovan Chakraborty. Supernova Neutrinos: Production, Oscillations and Detection. *Riv. Nuovo Cim.*, 39(1-2):1–112, 2016.

[3] W. D. Arnett, John N. Bahcall, R. P. Kirshner, and S. E. Woosley. SUPERNOVA SN1987A. *Ann. Rev. Astron. Astrophys.*, 27:629–700, 1989.

[4] Shirley Weishi Li, John F. Beacom, Luke F. Roberts, and Francesco Capozzi. Old data, new forensics: The first second of SN 1987A neutrino emission. *Phys. Rev. D*, 109(8):083025, 2024.

[5] Kate Scholberg. Supernova Neutrino Detection. *Ann. Rev. Nucl. Part. Sci.*, 62:81–103, 2012.

[6] Scott M. Adams, C. S. Kochanek, John F. Beacom, Mark R. Vagins, and K. Z. Stanek. Observing the Next Galactic Supernova. *Astrophys. J.*, 778:164, 2013.

[7] Jackson Olsen and Yong-Zhong Qian. Prospects for distinguishing supernova models using a future neutrino signal. *Phys. Rev. D*, 105:083017, Apr 2022.

[8] Z. P. Ye et al. A multi-cubic-kilometre neutrino telescope in the western Pacific Ocean. *Nature Astron.*, 7(12):1497–1505, 2023.

[9] Wei Zhi, Jie Zheng, Wei Tian, Donglian Xu, and Xin Xiang. Preliminary Design of the Hybrid Digital Optical Module for TRIDENT. *PoS*, ICRC2023:1213, 2023.

[10] A. Albert et al. Long-term monitoring of the ANTARES optical module efficiencies using ^{40}K decays in sea water. *Eur. Phys. J. C*, 78(8):669, 2018.

[11] S. Adrián-Martínez et al. Deep sea tests of a prototype of the KM3NeT digital optical module. *Eur. Phys. J. C*, 74(9):3056, 2014.

[12] F. Halzen, J. E. Jacobsen, and E. Zas. Ultratransparent Antarctic ice as a supernova detector. *Phys. Rev. D*, 53:7359–7361, 1996.

[13] R. Abbasi et al. IceCube Sensitivity for Low-Energy Neutrinos from Nearby Supernovae. *Astron. Astrophys.*, 535:A109, 2011. [Erratum: Astron.Astrophys. 563, C1 (2014)].

[14] R. Abbasi et al. Search for Galactic Core-collapse Supernovae in a Decade of Data Taken with the IceCube Neutrino Observatory. *Astrophys. J.*, 961(1):84, 2024.

[15] C. J. Lozano Mariscal, Cristian Jesús Lozano Mariscal, L. Classen, Lew Classen, M. A. Unland Elorrieta, Martin Antonio Unland Elorrieta, A. Kappes, and Alexander Kappes. Sensitivity of multi-PMT optical modules in Antarctic ice to supernova neutrinos of MeV energy. *Eur. Phys. J. C*, 81(12):1058, 2021. [Erratum: Eur.Phys.J.C 82, 660 (2022)].

[16] S. Aiello et al. The KM3NeT potential for the next core-collapse supernova observation with neutrinos. *Eur. Phys. J. C*, 81(5):445, 2021.

[17] V. N. Kondratyev, N. G. Khor'kova, and S. Cherubini. Supernova Neutrino Spectra and Observations by Large Volume Telescopes. *Phys. Atom. Nucl.*, 85(6):924–930, 2022.

[18] Y. Fukuda et al. The Super-Kamiokande detector. *Nucl. Instrum. Meth. A*, 501:418–462, 2003.

[19] P. C. de Holanda and A. Yu. Smirnov. Solar neutrinos: The SNO salt phase results and physics of conversion. *Astropart. Phys.*, 21:287–301, 2004.

[20] Alessandro Strumia and Francesco Vissani. Precise quasielastic neutrino/nucleon cross-section. *Phys. Lett. B*, 564:42–54, 2003.

[21] Irene Tamborra, Georg Raffelt, Florian Hanke, Hans-Thomas Janka, and Bernhard Mueller. Neutrino emission characteristics and detection opportunities based on three-dimensional supernova simulations. *Phys. Rev. D*, 90(4):045032, 2014.

[22] E. V. Bugaev, A. Misaki, Vadim A. Naumov, T. S. Sinegovskaya, S. I. Sinegovsky, and N. Takahashi. Atmospheric muon flux at sea level, underground and underwater. *Phys. Rev. D*, 58:054001, 1998.

[23] G. Carminati, A. Margiotta, and M. Spurio. Atmospheric MUons from PArametric formulas: A Fast GEnerator for neutrino telescopes (MUPAGE). *Comput. Phys. Commun.*, 179:915–923, 2008.

[24] Huang W. et al. The trigger and data acquisition system of the trident phase-i detector, June 2024.

[25] O. Adriani et al. The Online Data Filter for the KM3NeT Neutrino Telescopes. 6 2025.

[26] NNDC. Thermal neutron capture 's (capgam).

[27] Isabel Astrid Goos. Km3net's sensitivity to the next core-collapse supernova, June 2024.

[28] M. Mori et al. Searching for Supernova Bursts in Super-Kamiokande IV. *Astrophys. J.*, 938(1):35, 2022.

[29] Angel Abusleme et al. Real-time monitoring for the next core-collapse supernova in JUNO. *JCAP*, 01:057, 2024.

[30] Maria Manuela Saez, Ermal Rrapaj, Akira Harada, Shigehiro Nagataki, and Yong-Zhong Qian. Correlations and Distinguishability Challenges in Supernova Models: Insights from Future Neutrino Detectors. 1 2024.

[31] Papia Panda, Monojit Ghosh, and Rukmani Mohanta. Determination of neutrino mass ordering from Supernova neutrinos with T2HK and DUNE. *JCAP*, 10:033, 2023.

[32] N. B. Linzer and K. Scholberg. Triangulation Pointing to Core-Collapse Supernovae with Next-Generation Neutrino Detectors. *Phys. Rev. D*, 100(10):103005, 2019.